Vibrational Imaging with High Sensitivity via Epidetected Coherent Anti-Stokes Raman Scattering Microscopy

Andreas Volkmer, Ji-Xin Cheng, and X. Sunney Xie*

Department of Chemistry and Chemical Biology, Harvard University, 12 Oxford Street, Cambridge, Massachusetts 02138

(Received 24 December 2000; published 20 June 2001)

We demonstrate theoretically and experimentally a novel epidetection scheme for coherent anti-Stokes Raman scattering (CARS) microscopy that significantly improves the detection sensitivity. Calculations show that epidetected CARS (E-CARS) signals are present for scatterers smaller than the wavelength of light, whereas the large background signals from the surrounding bulk solvent are suppressed by destructive interference. E-CARS microscopy is capable of revealing small intracellular features that are otherwise buried by the strong water CARS signal.

DOI: 10.1103/PhysRevLett.87.023901 PACS numbers: 42.65.Dr, 42.65.Hw, 87.16.–b, 87.64.–t

Recent advances [1] in vibrational imaging based on coherent anti-Stokes Raman scattering (CARS) have attracted much interest [2–5]. In CARS, pump and Stokes incident electromagnetic fields with frequencies ω_P and ω_S, respectively, interact with a sample and generate an anti-Stokes signal field at $\omega_{AS} = 2\omega_P - \omega_S$ in the phase-matched direction. The signal is enhanced when the Raman shift, $\omega_P - \omega_S$, coincides with the frequency of a Raman active molecular vibration [6]. CARS microscopy is a particularly attractive approach to vibrational imaging of biological samples for the following reasons: First, vibrational contrast of CARS is inherent to chemical species, and thus requires no natural or artificial fluorophores that are prone to photobleaching. Second, the coherent nature of CARS offers a much higher sensitivity than spontaneous Raman microscopy, and necessitates significantly lower average excitation powers tolerable by most biological systems. Third, the nonlinear intensity dependence of CARS results in signal generation only from the focal volume and allows three-dimensional sectioning of thick samples with high spatial resolution, which is similar and complementary to two-photon fluorescence imaging [7]. In 1982, Duncan *et al.* first reported a CARS microscope, using noncollinear pump and Stokes beams and a two-dimensional detector to detect the anti-Stokes beam in the phase-matching direction [8]. Recently, Zumbusch *et al.* made a significant step toward confocal CARS microscopy with three-dimensional sectioning capability by tightly focusing collinearly propagating pump and Stokes beams, and detecting CARS in the forward direction [(F-CARS); see Fig. 1 for geometry] [1]. The efforts to increase CARS sensitivity, however, were impeded by the fact that the CARS signal is not free of solvent background. Because of electronic contributions to the third-order nonlinear susceptibility, there exists a nonresonant solvent CARS signal independent of Raman shifts [5]. In addition, the common solvent water has strong resonant signals with broad spectral widths. These solvent background signals often overwhelm CARS signals from small scatterers. In this paper, we demonstrate that, by detecting CARS in the backward direction [epidetected CARS (E-CARS); see Fig. 1 for geometry], one can suppress effectively the solvent background and increase significantly the sensitivity of CARS microscopy.

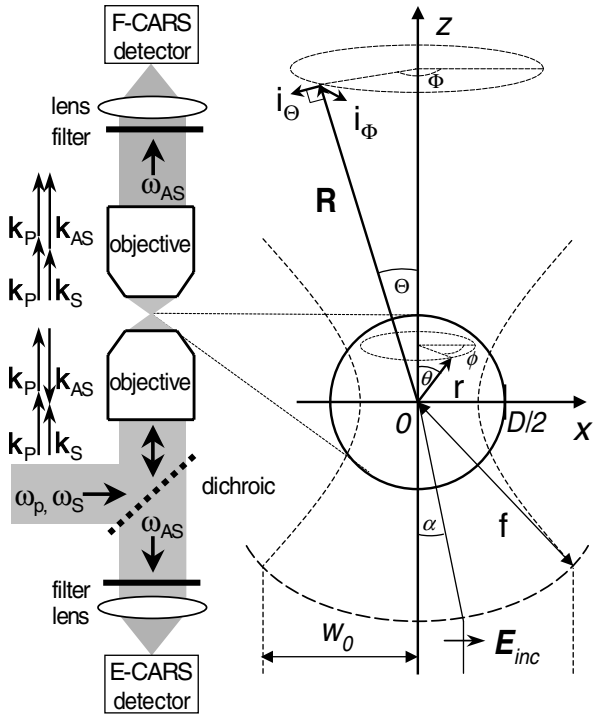

FIG. 1. Schematic of the configurations for F- and E-CARS microscopy with collinear pump and Stokes beams and confocal detection in the forward and backward directions, respectively. The zoom-in picture shows the definition of the parameters used in the calculation. Gaussian beams of pump and Stokes lights with beam waists of w_0 are focused by a high NA objective of f focal length, generating the CARS from a spherical sample of diameter D. The radiation field of the induced polarization, $P^{(3)}(\mathbf{r}, \omega_{AS})$, is integrated over the sample, and the detected F- and E-CARS intensities are calculated by integrating the Poynting vector at the far-field along the surface of constant R ($R \gg r$).

 © 2001 The American Physical Society

We first qualitatively describe the physical picture by assuming that the pump and Stokes beams are monochromatic plane waves propagating along the $\mathbf{z}$ axis through a sample slab of thickness D. The anti-Stokes emission generated in the slab propagates in the forward (along $\mathbf{z}$) and the backward (along $-\mathbf{z}$) directions with intensities being [6,9]

$$I_{AS}(D) = \frac{\pi}{2n_{AS}c}\,\omega_{AS}^2 D^2 |\mathbf{P}^{(3)}|^2\,\mathrm{sinc}^2\!\left(\frac{|\Delta\mathbf{k}|D}{2}\right), \quad (1)$$

where $\mathbf{P}^{(3)}$ is the third-order polarization, c is the vacuum velocity of light, n_{AS} is the refractive index at the anti-Stokes angular frequency ω_{AS}, and $\mathrm{sinc}(x) = \sin(x)/x$. The phase mismatch is given by $\Delta\mathbf{k} = \mathbf{k}_{AS} - (2\mathbf{k}_P - \mathbf{k}_S)$, where $\mathbf{k}_P$, $\mathbf{k}_S$, and $\mathbf{k}_{AS}$ represent the wave vectors of the pump, Stokes, and anti-Stokes fields ($|\mathbf{k}_j| = 2\pi n_j/\lambda_j$, $j = P, S, AS$, λ_j being the vacuum wavelength). The phase-matching condition is $|\Delta\mathbf{k}|D \ll \pi$. It is important to realize that for a very thin slab, $D \approx 0$, the phase-matching condition is satisfied in both the forward ($\mathbf{k}_{AS}$ along $\mathbf{z}$) and backward ($\mathbf{k}_{AS}$ along $-\mathbf{z}$) directions. Consequently F-CARS and E-CARS are equal in intensity. With increasing D, however, the forward signal starts to overwhelm the backward signal because of the constructive interference in the forward direction and the destructive interference in the backward direction.

If the dispersion of the refractive index is negligible ($n = n_{AS} = n_P = n_S$), the F-CARS signal ($|\Delta\mathbf{k}| = 0$) has a quadratic dependence on D, $I_{AS}^F(D) \propto D^2$. Therefore, contribution to the signal from the solvent (large D) can overwhelm the contribution from a thin sample (small D). In the case of E-CARS ($|\Delta\mathbf{k}| = 4n\pi/\lambda_{AS}$), the signal oscillates as a function of D with a periodicity of $\lambda_{AS}/2n$, $I_{AS}^E(D) \propto \lambda_{AS}^2 \sin^2(2\pi n D/\lambda_{AS})$. Therefore, the solvent contribution (large D) is significantly reduced compared to that of F-CARS. Bearing in mind that a thin sample has equal E-CARS and F-CARS, this is the basis for increasing the signal-to-background ratio for E-CARS microscopy. A similar approach suppressing nonresonant background from the bulk in sum-frequency generation has been reported [10].

In reality, the tightly focused incident beams rather than plane waves are used. The former can be viewed as a superposition of plane waves. However, the physical picture described above remains the same. We now quantitatively evaluate the F-CARS and E-CARS signals for tightly focused beams. Richards and Wolf described the focal fields of tightly focused plane waves in 1959 [11]. Novotny [12] recently extended the approach to describe the focal field of tightly focused Gaussian beams [13]. Accordingly, we assume that the incident beams propagate along the optical axis $\mathbf{z}$ and are linearly polarized along the $\mathbf{x}$ axis. They are focused by a lens of the focal length f and a numeric aperture $\mathrm{NA} = n\sin\alpha_{\max}$, $\alpha_{\max}$ being the maximum cone angle α, as depicted in Fig. 1. The beams have Gaussain profiles with beam waists of w_0 before the lens, $E_j^{\mathrm{inc}} = E_{j0}\exp(-f^2\sin^2\alpha/w_0^2)$, with $j = P, S$ for the pump and Stokes fields, respectively. Near the tight focus, the field distribution is no longer Gaussian because of the breakdown of the paraxial approximation. The y and z components of the fields near the focus are relatively small and can be neglected. The x component of the focal fields in cylindrical coordinates is given by [12]

$$E_j(\rho, z) = \frac{1}{2}\,ik_j f e^{-ik_j f}\int_0^{\alpha_{\max}} E_j^{\mathrm{inc}}\sqrt{\cos\alpha}\,(1+\cos\alpha) \times J_0(k_j\rho\sin\alpha)\sin\alpha\, e^{ik_j z\cos\alpha}\,d\alpha\,, \quad (2)$$

with $\rho = \sqrt{x^2 + y^2}$, and J_0 being the zero-order Bessel function.

We now place a spherical sample with diameter D at the origin of the overlapped foci of the pump and Stokes beams. We make an important and convenient approximation that the refractive index mismatch between the sample and the solvent is negligible. Therefore, the incident fields are unperturbed by the presence of the sample. We also assume $n = n_{AS} = n_P = n_S$ [14]. Under the assumption of undepleted excitation, the incident fields induce a third-order polarization, $P^{(3)}(\mathbf{r}, \omega_{AS})$, of the sample at the anti-Stokes frequency, ω_{AS},

$$P^{(3)}(\mathbf{r}, \omega_{AS}) = \chi^{(3)}(\omega_{AS})E_P^2(\mathbf{r})E_S^*(\mathbf{r})\,, \quad (3)$$

where $\chi^{(3)}(\omega_{AS})$ is the third-order susceptibility, and $E_P(\mathbf{r})$ and $E_S(\mathbf{r})$ represent the focused pump and Stokes fields polarized along $\mathbf{x}$, as described by Eq. (2).

We determine the CARS radiation field per unit sample volume, $\vec{\mathcal{E}}_{AS}(\mathbf{R}, \mathbf{r}, \omega_{AS})$, by calculating the Hertzian radiation field of the induced polarization, $\mathbf{P}^{(3)}$, at $\mathbf{r} = \mathbf{r}(r, \theta, \phi)$ (see Fig. 1). In the far field, $|\mathbf{R}| \gg |\mathbf{r}|$, the radiation field generated at the $\mathbf{r}$ position assumes the following form [15,16]:

$$\vec{\mathcal{E}}_{AS}(\Theta, \Phi, \mathbf{r})dV = \frac{\omega_{AS}^2}{c^2}\,\mathbf{P}^{(3)}(\mathbf{r}, \omega_{AS})\,\frac{e^{i(k_{AS}R - k_{AS}\mathbf{R}\cdot r/R)}}{R} \times (\cos\Theta\cos\Phi\,\mathbf{i}_\Theta - \sin\Phi\,\mathbf{i}_\Phi)dV\,, \quad (4)$$

where Θ and Φ are the spherical coordinates specified by the vector $\mathbf{R}(R, \Theta, \Phi)$ (see Fig. 1). The unit vectors $\mathbf{i}_\Theta$ and $\mathbf{i}_\Phi$ denote transverse components orthogonal to $\mathbf{R}$.

The CARS field is the coherent summation of the radiation field of the induced polarization generated within the sample,

$$\mathbf{E}_{AS}(\Theta, \Phi, D) = \int_0^{2\pi} d\phi \int_0^{\pi} d\theta \int_0^{D/2} dr \times \vec{\mathcal{E}}_{AS}(\Theta, \Phi, \mathbf{r})r^2\sin\theta\,. \quad (5)$$

The radiation power from the scatterer, p_{CARS}, is calculated by integrating the Poynting vector over the cone angle ($\Theta_1 < \Theta < \Theta_2$) along the spherical surface of constant R,

$$p_{\mathrm{CARS}}(D) = \frac{cn}{8\pi}\int_{\Theta_1}^{\Theta_2} d\Theta \int_0^{2\pi} d\Phi |\mathbf{E}_{AS}(\Theta,\Phi,D)|^2 R^2 \times \sin\Theta\,, \quad (6)$$

where the integration range $[\Theta_1, \Theta_2]$ is $[0, \alpha_{\max}]$ for F-CARS and $[\pi - \alpha_{\max}, \pi]$ for E-CARS.

The E-CARS and F-CARS signals, as a function of diameter D, are plotted in Fig. 2(a). The F-CARS signal increases quasiquadratically with D and becomes saturated when D exceeds the longitudinal dimension of the focal excitation volume, i.e., full width at half maximum (FWHM) $\sim$1.2 μm for the experimental condition. The E-CARS signal, however, appears only for small spheres and exhibits several maxima, with the highest one at $\sim 0.65\lambda_P$, and a periodicity close to that under the plane wave condition ($\lambda_{AS}/2n$). The E-CARS signal intensity is negligible for large D, which resembles the case of focusing into an isotropic bulk medium. The ratio of E-CARS and F-CARS as a function of D [Fig. 2(b)] quantitatively proves the presence of the E-CARS signal for small scatterers under the tightly focused condition.

The F-CARS and E-CARS detection schemes, as shown in Fig. 1, were experimentally implemented. A regeneratively amplified Ti:sapphire laser system that pumped an optical parametric amplifier (RegA 9000/OPA 9400, Coherent) and operated at a repetition rate of 250 kHz was used to provide femtosecond pulses (FWHM $\sim$110 fs) for the excitation fields. Both linearly polarized pump and Stokes beams were temporally overlapped by an optical delay line, collinearly sent into an inverted optical microscope (Nikon TE 300) and focused with an oil-immersion objective lens (Nikon Plan Apo, 60×, NA = 1.4). The E-CARS and F-CARS signals were spectrally filtered and confocally detected by avalanche photodiodes (SPCM-APD 200, EG&G Canada). CARS images were collected by raster scanning the sample, respective to the fixed laser beams, using a closed-loop piezo-driven scanner (Physik Instrumente).

We used polystyrene beads (Polysciences, $D = 535 \pm 10$ nm) spin coated on a glass cover slip and covered with water, as test samples. Figures 3(a) and 3(b) depict the lateral profile of the F- and E-CARS signals of a bead, which were recorded simultaneously. The CARS signals were proved by the quadratic and the linear dependence of the signal on the pump and Stokes intensities, respectively. Because of the broad spectral bandwidth of the femtosecond excitation pulses (FWHM $\sim$300 cm^{-1}), the measured signal originates from several bands of polystyrene, i.e., the C—H bending (1447 cm^{-1}) and C═C stretching (1582 cm^{-1} and 1602 cm^{-1}) vibrations. Imaging with a higher spectral resolution has been demonstrated with a picosecond system [5].

Figure 3 clearly demonstrates the efficient rejection of solvent signal and a significant increase of sensitivity in E-CARS microscopy. The signal-to-background ratio for F-CARS [Figure 3(a)] amounts to $\sim$1.5, whereas that for E-CARS profile [Figure 3(b)] is >20. It was found that the E-CARS of pure water is more than a factor of 100 smaller than the simultaneously measured F-CARS, which is consistent with the calculation in Fig. 3(b). Interestingly, two dips are observed in the lateral F-CARS profile [Fig. 3(a)]. The phenomenon might arise from destructive interference between the F-CARS of the sample and the solvent, which will be discussed in detail elsewhere [17].

It should be noted that the refractive index mismatch between the sample and the solvent, which is not considered in the calculation, can cause backreflection of F-CARS. For example, the remaining nonzero E-CARS for $x < 1$ μm and $x > 2$ μm in the intensity profile [Fig. 3(b)] is the F-CARS from the glass substrate ($n = 1.52$) backreflected by the glass-water interface. The signal disappears when water ($n = 1.33$) is replaced with index-matching oil ($n = 1.51$). In practice, if the beams are not focused on an interface, the backreflected F-CARS is defocused, and can be minimized by using confocal detection. If the size of the scatterer is small, the backreflected F-CARS signal is negligible. For larger scatterers, however, backreflected

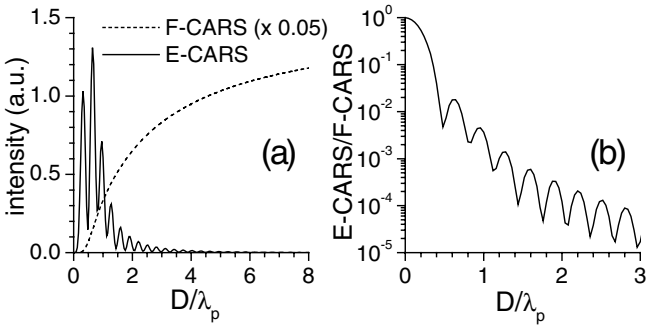

FIG. 2. Calculations of the F- and E-CARS intensities for tightly focused excitation beams: (a) F- and E-CARS intensity and (b) the ratio of E-CARS/F-CARS as a function of sphere diameter D. The pump and Stokes wavelengths are at λ_P = 800 nm and λ_S = 917 nm, respectively. The index of refraction of the medium is 1.52 and the NA of the lens is 1.4.

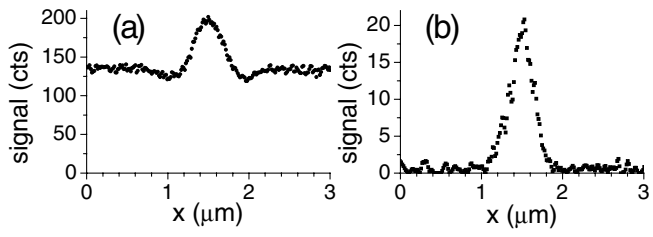

FIG. 3. Measured lateral (a) F-CARS and (b) E-CARS intensity profiles of a polystyrene bead with 535 nm diameter on a glass cover slip and covered with water. Pump and Stokes wavelengths are at 800 and 917 nm (Raman shift centered at $\sim$1600 cm^{-1}), with average powers of 50 and 25 μW, respectively. The integration time per pixel is 4.88 ms. The FWHM of the F- and E-CARS intensity profile amounts to 300 ± 10 nm and 290 ± 10 nm, respectively.

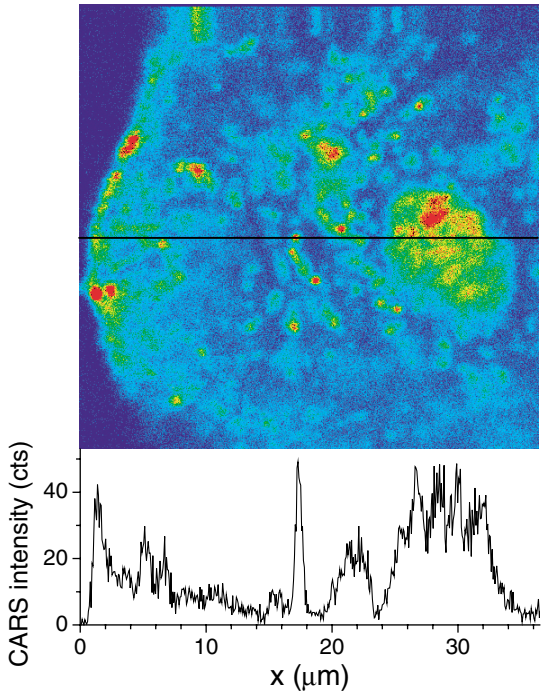

FIG. 4. E-CARS image of an unstained human epithelial cell in an aqueous environment. The image was taken with 50 and 25 μW average powers of the pump and Stokes beams at 741 and 800 nm, respectively, corresponding to a Raman shift of 1000 cm^{-1}. The image size amounts to 512×512 $(pixel)^2$ with an integration time of 4.88 ms per pixel. The lateral intensity profile along the black line indicates the efficient rejection of the aqueous solvent signal (see the $x < 0.5$ μm region), and the identification of small features (FWHM of 550 ± 50 nm at $x = 17.3$ μm).

F-CARS can be used as an additional contrast mechanism in epidetection.

E-CARS imaging of an unstained epithelial cell in an aqueous environment was demonstrated in Fig. 4. The Raman shift is 1000 cm^{-1}, characteristic for C—O stretching vibrations of DNA [18]. The image contrast vanishes when the pump and Stokes pulses were not temporally or spatially overlapped. The cell nucleus with apparent substructure and the diffraction-limited features within the cytoplasm are clearly visible, which could not be seen with the F-CARS detection.

We have provided theoretical and experimental proof of principle for E-CARS microscopy, which dramatically increases the sensitivity of CARS detection for scatterers smaller than the wavelength of light. This method is particularly useful for intracellular imaging. It should be noted that the concept of engineering the phase-matching condition in order to extract the small signal from the huge solvent background is generally applicable to other nonlinear coherent microscopy, such as second harmonic generation [19] and third harmonic generation [20]. E-CARS can be easily implemented with a commonly used epifluorescence microscope and provides a superior sensitivity for a point-by-point chemical map of living cells with vibrational spectroscopy.

The authors acknowledge Dr. Lukas Novotny for helpful discussions and for sharing Ref. [12] prior to its publication. We also thank Dr. Erik J. Sanchez for the data acquisition software, Dr. Lewis D. Book and John T. Krug II for many helpful discussions and comments on the manuscript. The Faculty of Arts and Sciences of Harvard University supported this work. A. V. acknowledges support from the Deutsche Forschungsgemeinschaft (DFG).

*Corresponding author.
Email address: xie@chemistry.harvard.edu

[1] A. Zumbusch, G. R. Holtom, and X. S. Xie, Phys. Rev. Lett. **82**, 4142 (1999).
[2] M. Müller, J. Squier, C. A. d. Lange, and G. J. Brakenhoff, J. Microsc. **197**, 150 (2000).
[3] E. O. Potma, W. P. d. Boeij, and D. A. Wiersma, J. Opt. Soc. Am. B **17**, 1678 (2000).
[4] M. Hashimoto, T. Araki, and S. Kawata, Opt. Lett. **25**, 1768 (2000).
[5] J.-X. Cheng, A. Volkmer, L. D. Book, and X. S. Xie, J. Phys. Chem. B **105**, 1277 (2001).
[6] Y. R. Shen, *The Principles of Nonlinear Optics* (Wiley, New York, 1984), p. 49.
[7] W. Denk, J. H. Strickler, and W. W. Webb, Science **248**, 73 (1990).
[8] M. D. Duncan, J. Reintjes, and T. J. Manuccia, Opt. Lett. **7**, 350 (1982).
[9] S. Mukamel, *Principle of Nonlinear Optical Spectroscopy* (Oxford University Press, New York, 1995), p. 98.
[10] X. Wei, S. C. Hong, A. I. Lvovsky, H. Held, and Y. R. Shen, J. Phys. Chem. B **104**, 3349 (2000).
[11] B. Richards and E. Wolf, Proc. R. Soc. London A **253**, 358 (1959).
[12] L. Novotny, *Lecture Notes on Nano-optics* (University of Rochester, Rochester, NY, 2000).
[13] This treatment deals with continuous wave excitation. Although femtoscond pulses are used, their spatial width exceeds the focal interaction length. Therefore, the incident fields can be treated as quasi-cw ones.
[14] We verified that the dispersion of the refractive indices causes negligible wave vector mismatch because of the small excitation volume under the tight focus condition.
[15] L. Novotny, J. Opt. Soc. Am. A **14**, 105 (1997).
[16] J. D. Jackson, *Classical Electrodynamics* (Wiley, New York, 1975), p. 395.
[17] J.-X. Cheng, A. Volkmer, L. D. Book, and X. S. Xie (to be published).
[18] G. J. Puppels, in *Fluorescent and Luminescent Probes for Biological Activity,* edited by W. T. Mason (Academic Press, New York, 1999), 2nd ed., p. 377.
[19] J. N. Gannaway and C. J. R. Sheppard, Opt. Quantum Electron. **10**, 435 (1978).
[20] Y. Barad, H. Eisenberg, M. Horowitz, and Y. Silberberg, Appl. Phys. Lett. **70**, 922 (1997).